International Journal of Research in Engineering and Science (IJRES)
ISSN (Online): 2320-9364, ISSN (Print): 2320-9356
www.ijres.org Volume 9 Issue 9 ‖ 2021 ‖ PP. 86-94

Research on Flow Field and Aerodynamic Characteristics of H-type Vertical Axis Wind Turbine under Different Tip Speed Ratio

Zhang Yanfeng[1], Zhu Xinyu[2], Song Xiaowen[2], Guo Zhiping[2*]
[1]College of Science, Inner Mongolia University of Technology, Hohhot, CHINA
*[*2]College of Mechanical Engineering, Inner Mongolia University of Technology, Hohhot 010051, CHINA*
*Corresponding Author:Guo Zhiping*1666061738@qq.com

Abstract
Analyzing and predicting the flow field and aerodynamic performance of H-type vertical axis wind turbine (VAWT), and attaching importance to the phenomenon of dynamic stall, can improve its adaptability to high-turbulence complex cities and remote areas far away from the power grid. According to the structural characteristics of the H-type vertical axis wind turbine, the blade element is subjected to force analysis by using the blade element-momentum theory. The power coefficients of the VAWT are compared and analyzed between computational fluid dynamics (CFD) simulations and wind tunnel experiment to estimate the validity of simulation results. This study focuses on the associated feature of flow field and aerodynamic characteristics of H-type VAWT under different tip speed ratios (TSRs). As a result, the dynamic stall directly affects the aerodynamic performance of VAWT at low TSR, which results in lower power output of blades. Th better mechanical property of VAWT is occurred at high TSR, that has similar instantaneous pressure distributions on blades surface and the aerodynamic forces of the rotor shaft. The above research work provides the calculation model and theoretical basis for predicting flow field and improving aerodynamic performance of wind turbine.
Keywords:*Vertical Axis Wind Turbine, CFD, tip speed ratio, flow field, aerodynamic characteristics.*

Date of Submission: 13-09-2021 Date of acceptance: 28-09-2021

I. INTRODUCTION

With the rapid growth of economic growth and energy consumption, fossil energy is gradually reduced, which forces governments around the world to vigorously develop alternative clean energy [1, 2]. As a clean, economical, sustainable and abundant renewable energy source, wind energy has been favored by governments and large energy companies [3]. Therefore, the research into improving the overall performance of wind turbines has become a hot research field [4, 5].

In recent years, the application of Vertical Axis Wind Turbine (VAWT) in cities and remote mountain areas has attracted more and more attention [6]. H-type VAWTs can work downward in different incoming wind, have higher adaptability and low noise level to turbulent or oblique flow, in which has better adaptability and output characteristics than HAWT [7]. At present, it is still a research hotspot in this field to explore the regularity of flow field and aerodynamic characteristics of specific airfoil under different geometric parameters and seek to improve VAWT power performance [8, 9].

At present, wind tunnel experiment and numerical simulation are the main methods to study the flow field and aerodynamic characteristics of wind turbines [10-12]. Li Q et al. used wind tunnel and simulation to predicting aerodynamic loads and performance of a straight-bladed VAWT [13, 14]. The winglet for vertical axis wind turbines was designed to decrease the tip vortex in the flow field based on experiment and CFD approach [15]. Elkhoury M et al. assessed the effects of inlet velocity, turbulence intensity, airfoil profile and variable-pitch on the performance of the VAWT by experimental and numerical investigation [16]. Li Q et al. used flow tube method and LDV test method to find that the energy absorbed by the wind turbine mainly comes from the work done by the blades in the upstream domain, meanwhile, the data indicated that the increase of Reynolds number can improve the power performance of the wind turbine [17]. It can be found by wind tunnel experiment that high turbulence is conducive to rapid wake recovery, and the change of turbulence intensity has little influence on the output power at low tip speed ratio TSR [18].

In the process of numerical simulation of VAWTs, the mesh quality, the time step and the turbulence intensity have caused significant differences in the flow field distribution and output characteristic predicting, which if not considered the problem all sidedly could lead to unreliable analysis result [19, 20]. Almohammadi K et al. studied the influence of wall conditions, mesh shape and time step on the calculation results of wind turbine in CFD, and found that quadrilateral mesh has higher accuracy [21]. A sliding mesh was employed to research the interaction between aerodynamic characteristics and flow separation, and power and torque considering the rotational effect of the blades [22, 23]. Wekesa DW et al. used a steady wind simulation model to predict the power performance for the VAWTs [24, 25]. By means of CFD simulation and design modifications, it could be found the straight-bladed VAWTs with symmetrical airfoil (NACA 0012, NACA 0015) have better flow field and aerodynamic characteristics in results, such as lift force, velocity, and tangential force [26]. The performance of flow effects physics on blade tip, spanwise flow, support arm and rotor shaft were analyzed respectively with the help of CFD [27].

In summary, researchers have achieved significant in the study of the influence of structural parameters and wind speed on the flow field and aerodynamic characteristics of the H-type VAWT. However, there are few studies on the influence of the flow field and aerodynamic characteristics of the blade section position on the torque and power performance of the of VAWTs at different TSRs. Therefore, the main purpose of this paper is to study the flow field and aerodynamic load of wind turbine blade section by using CFD simulations, reveal the associated feature of flow field and aerodynamic characteristics of H-type VAWT under different TSRs, and provide theoretical support for optimizing blade section parameters and improving VAWT power performance.

II. H-type VAWT structure

The H-type vertical axis wind turbine is mainly composed of wind wheel, power generation system, braking system and other auxiliary systems. As shown in Fig.1, the wind wheel is composed of blade, support arm and rotary shaft.

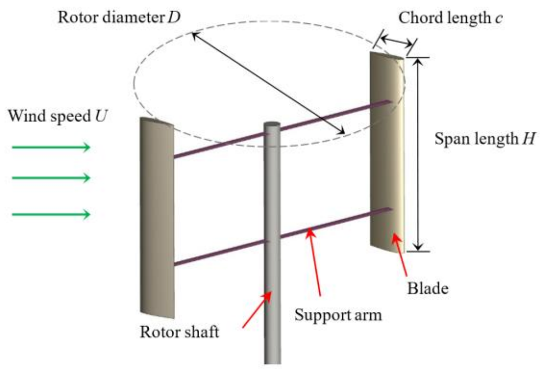

Fig.1 H-type VAWT structure

Because the H-type VAWT is of constant cross-section design, the blade of the wind turbine is divided into many equivalent micro-segments along the wingspan according to the blade element theory. As shown in Fig.2, the incoming wind speed U is from left to right, and the tip speed of blade V is the blade tangential velocity. The resultant flow velocity$\boldsymbol{W}$ is

$$\boldsymbol{W}=\boldsymbol{U}+\boldsymbol{V} \quad (1)$$

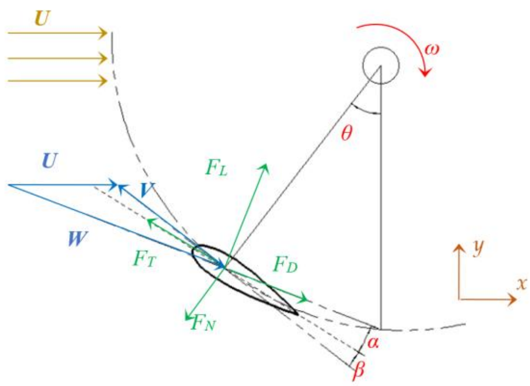

Fig.2 Blade force analysis

The component F_x of the aerodynamic force in the x direction is the thrust force, and the component F_y in the y direction is the lateral force. F_x andF_y are decomposed into the tangential force (F_T) along the chord direction and the normal force (F_N) perpendicular to the chord direction. Then

$$F_T = F_y \cdot \sin\theta - F_x \cdot \cos\theta\ ,\ F_N = -F_y \cdot \cos\theta - F_x \cdot \sin\theta \quad (2)$$

The lift force (F_L) direction of the wind turbine blade is perpendicular to the direction of the blade resultant flow velocity (W), and the draft force (F_D) direction of the blade coincides with the direction of W, then

$$F_L = F_T \cdot \cos\varphi - F_N \cdot \sin\varphi\ ,\ F_D = -F_T \cdot \sin\varphi - F_N \cdot \cos\varphi \quad (3)$$

where φ is the angle of resultant flow velocity, the φ equals the angle of attack(α) plus is the blade pitch angle (β).

In order to better describe the aerodynamic characteristics of the wind turbine blade, the abovementioned various loads are dimension processed to obtain the load factor as shown in Tab.1.

Tab.1 Dimension load factor

Load type	Formula	Load type	Formula
Tip speed ratio (TSR)	$\lambda=R\ \omega/U_0$	Thrust coefficient	$C_{TH}=F_x/0.5\rho cHU_0^2$
Normal force coefficient	$C_N=F_N/0.5\rho cHU_0^2$	Tangential force coefficient	$C_T=F_T/0.5\rho cHU_0^2$
Lift coefficient	$C_L=F_L/0.5\rho cHU_0^2$	Draft coefficient	$C_D=F_D/0.5\rho cHU_0^2$
Torque coefficient	$C_Q=Q/0.5\rho AU_0^2R$	Power coefficient	$C_{power}=Q\omega/0.5\rho DAU_0^3$

In Tab.1, ρ is the air density (kg/m^3), U_0 is the incoming wind speed (m/s), and R is the radius of gyration ($R=D/2$), ω is the angular velocity of rotor shaft (rad/s), ω is the wind wheel angular velocity (rad/s), A is the windward area of the wind turbine ($A=D\cdot H$, m^2).

III. Numerical model

3.1 Physical Model

This paper's main purpose is to research on flow field and aerodynamic characteristics of H-type VAWT under different tip speed ratio. Thus, a small straight-bladed VAWT is researched, which is utilized in a published paper [14,17]. The basic parameters of the VAWT model are listed in Tab.2, and the rotor's rotation direction and the blade's rotation angle are provided in Fig.2.

Tab.2 Parameters of H-type VAWT

Parameter	Value	Parameter	Value
Blade airfoil	NACA0021 (Fig.3)	Pitching angle (β)	6°
Blade number (N)	2	Rotor diameter (D)	2.000 m
Span length (H)	1.2 m	Shaft diameter (d)	0.15 m
Chord length (c)	0.265 m	Shaft length (h)	1.2 m

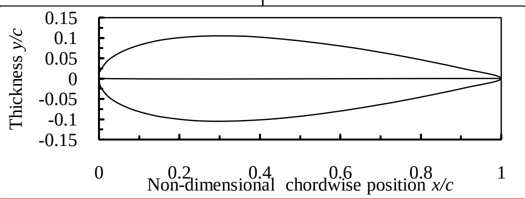

Fig.3 Airfoil of the test blade

3.2 Computational domain & mesh setup

In order to simulate the flow field and aerodynamic characteristics of the wind turbine, the structured grid approach is adopted for the simulations. The computational domain can be divided into a resting outer zone and a rotating inner zone, those sizes are presented in Fig.4(a) by the rotor diameter D and blade span H. In the present study, the diameter of the inner zone is $2D$ and its height is $1H$. For the outer zone, its length is $20D$ in x-axis direction, its width is $10D$ in y-axis direction, while its height is $2H$ in z-axis direction. The gyration center of inner zone, is also the origin of coordinate system, is defined at 5*D* to the velocity inlet boundary of upstream domain and 15*D* to the pressure outlet boundary of downstream domain.

The mesh setup is completed in ANSYS ICEM CFD which contains components of meshing, calculating and post-processing. A variety of structured cells are employed in different zones. Fig.4(c) shows the prismatic boundary layer on the surface of the blades. Due to the large gradient of wind speed and pressure near the blades, the grid on the blade surface is densified to improve the calculation accuracy. The thickness of the first boundary layer is 0.02mm with a growth ratio of 1.25.

A uniform velocity profile (U_0=8m/s) is set as the inlet condition and the outlet boundary is considered as pressure outlet with zero relative pressure. The turbulence intensity is set as 1% and the value of turbulent length scale is 0.014mm in the inlet. The slip wall condition is assigned to the remaining four boundaries of the outer zone while the non-slip wall condition is assigned to blade and rotating shaft surfaces. The grid sizes and the number of grids of two zones in the contact interface must be guaranteed to be the same to exchange data efficiently and smoothly, in this way, which ensures the effectiveness of subsequent simulation analysis.

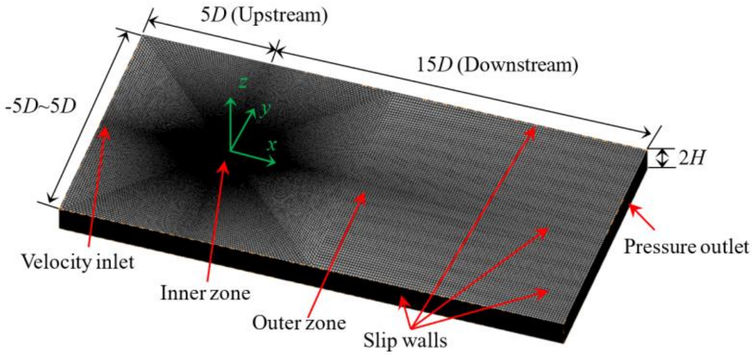

(a) 3D view of the computational domain

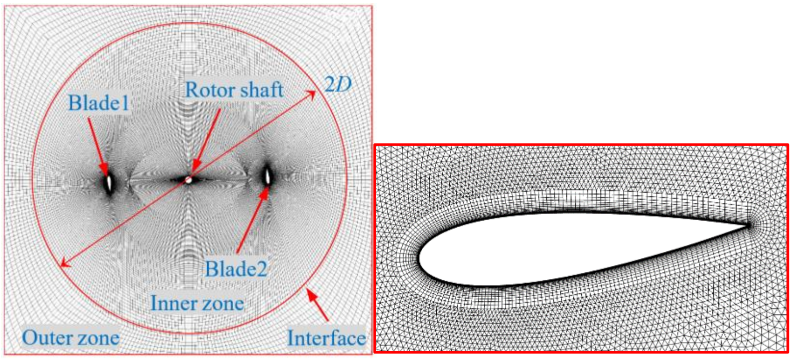

(b) Rotating domain grid(c) Blade surface boundary layer

Fig.4 Plan view of the computational domain with sizes

3.3 Solver setting

When the wind turbine rotates stably, the air flow on the blade surface is separated, and the air flow velocity is lower than 0.3 Mach, which means airflows can be considered to be an incompressible gaseous fluid in computational domain. The Shear Stress Transport (SST) k-ω turbulence model, treating flexibly wall boundaries and stabilising efficiently results, is employed to deal with boundary layer flow and revise turbulence formula. Taking in account the unsteady implicit segregated flow model and solving the discrete differential equations, the Semi-Implicit Method for Pressure Linked Equations (SIMPLE) is adopted to solve the problem of pressure-velocity coupling. When the residuals are equal to or lower than 10-3, the simulation schemes are confirmed deemed to be convergent.

IV. Results and discussions

4.1 Comparison of output characteristic

The output characteristic of instantaneous torque coefficient (C_Q) and power coefficient for single blade are discussed at different λ in this section. As shown in Fig.5(a), the change trend of the three C_Q curves are basically coincident over one revolution. The maximum value of $C_Q$are 0.37, 0.32 and 0.30, for λ=1.38, 2.19 and 2.58, which occur respectively at azimuth angle θ=105°, 110° and 115°. The maximum value occurs later during one rotational period when the tip speed ratio is larger. It can be found that the value of C_Q at each azimuth angle creates smaller variations for λ=2.19 and 2.58, which means that the torque of wind turbine changes significantly with the increase of tip speed ratio at U_0=8m/s.

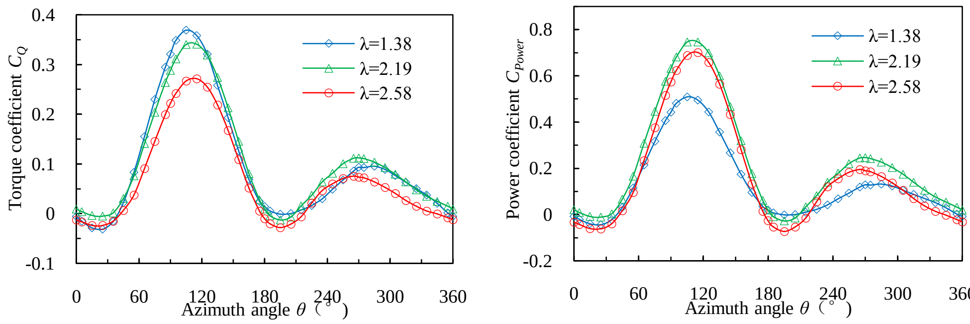

(a) Torque coefficient (b) Power coefficient

Fig.5 The instantaneous output characteristic for single blade

In Fig.5(b), a comparison instantaneous power performance during one rotational period is conducted. The power coefficient for one blade are all presented as positive values when azimuth angle falls into the interval between [45°, 175°] in upstream domain and [220°, 345°] in downstream domain. For comparing the power curves at different λ, the tow peak values are distributed in the upstream and the downstream domain respectively, which are focused on the size and location of the peak. It is obvious in upstream domain that the sizes of peak power are 0.51 at θ=105°, 0.75 at θ=110°and 0.70 at θ=115° for λ=1.38, 2.19 and 2.58. Moreover, the sizes of peak power in downstream domain are 0.13 at λ=1.38, 0.245 at λ=2.19, 0.20 at λ=2.58, and the locations are θ=285°, θ=270°and θ=265°. The peak power in upstream domain occurs later with the increase of λ. Nevertheless, the peak power in downstream domain appears earlier when the λ is larger.

4.2 Comparison of pressure distribution

Pressure distribution contours on the surfaces f one blade are analyzed with Fig.6 at the position of θ=90° where the maximum difference value of peak torque coefficient occurs. When θ=90° in upstream, the airflow directly acts on the outer side of the blade, the leeward side is the suction side of the blade while the upwind side is pressure side. In Fig.6 (a), on the pressure side of the blade, the value of pressure increases sharply from -450Pa at the leading edge to 60Pa at the position of 0.15*c* and then keeps at 60Pa to the trailing edge. The pressure always keeps negative on the suction side of the blade at λ=1.38. The absolute value of pressure decreases from 650Pa at the leading edge to 120Pa at the position of 0.2*c* and keeps at 120Pa to the position of 0.8*c*, then decreases to 0Pa at the trailing edge. In terms of the rate of pressure change. The changing rate of pressure is large between the leading edge and the position of 0.15*c* while the rate becomes relatively small after that. In Fig.6 (b) and (c), the pressure on the suction side of blade always keeps negative while the pressure on the pressure side of blade always keeps positive. The pressure developing tendency of blade is very similar at between λ=2.19 and λ=2.58. On the pressure side of the blade at λ=2.19 and 2.58, the value of pressure decreases respectively from 120Pa and 150Pa at the leading edge to 60Pa at the position of 0.2*c* and then all keeps at 60Pa to the trailing edge. On the suction side of the blade at λ=2.19 and 2.58, the absolute value of pressure decreases gradually from 850Pa and 600Pa at the leading edge to 0Pa at the trailing edge.

4.3 Comparison of vorticity field

As discussed above, when the profile of the blade is determined, the azimuth change leads to the variation of power coefficient and influences the vorticity field on the blade. the variation is not obvious and the small-scale vortices could not be captured very precisely. The vorticity fields of three cases at certain azimuthal angles interval 60°) are shown in Fig.7, that illustrates the tendency of vorticity development around one blade. Thus, the variation of vorticity is not very detailed and some vortices are too small-scale to be shown very precisely.

For λ=1.38, a large-scale separated vortex can be found on the outer side of blade and starts to slowly sheds at θ=0°. In the azimuth section [0°, 180°], the position of separated flow on the inner side moves from trialing edge to leading edge, and the moving direction of the air separation position on the inner side is exactly the opposite. A large-scale bound vortex occurs at the position of 0.3c on the inner side of blade and sheds from blade surface at θ=210°. A large- scale vortex is observed to form at the position of 0.4c on the outer side of blade surface at θ=270° and totally sheds from the blade surface at θ=330°. For λ=2.19 and 2.58, the trend of flow development is highly consistent at same azimuths. The growing vortex occurs in the outer side of blade surface towards the trailing edge at θ=0°and becomes extremely elongated at around θ=60°. The elongatedvortex starts to convert to the inner side at θ=90° and gets shorter at around θ=180°. In the azimuth section [180°, 330°], the growing elongatedvortex is always attached at the trailing edge of the blade, and the extension length of vortex in case of λ=2.58 is slightly longer than that in case of λ=2.19 at the same azimuth.

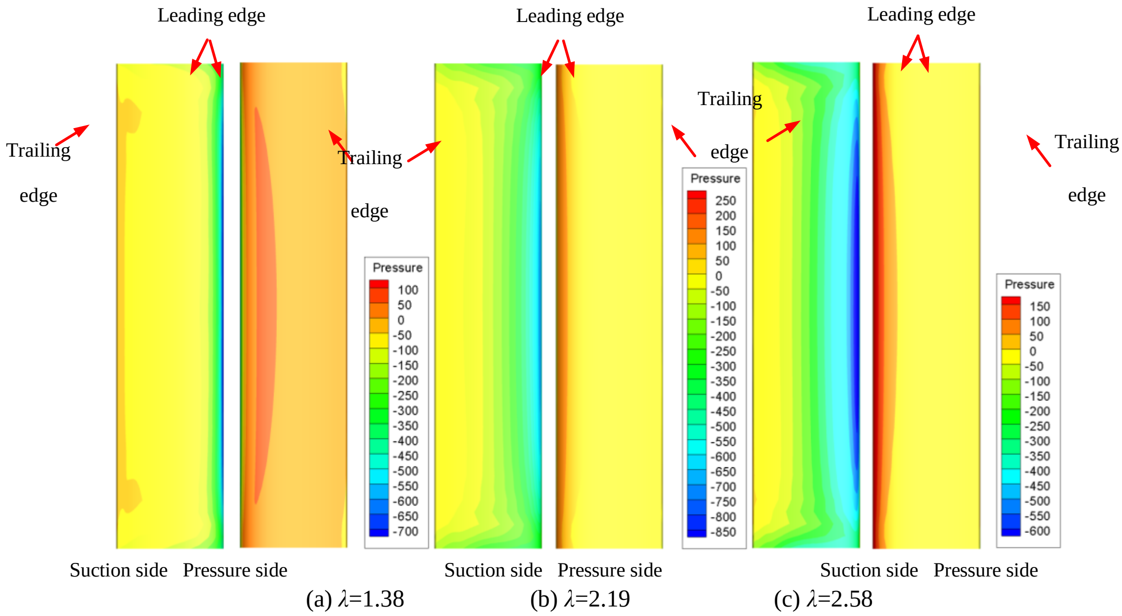

Fig.6 The pressure distribution on the surface of one blade at θ=90° (Unit: Pa)

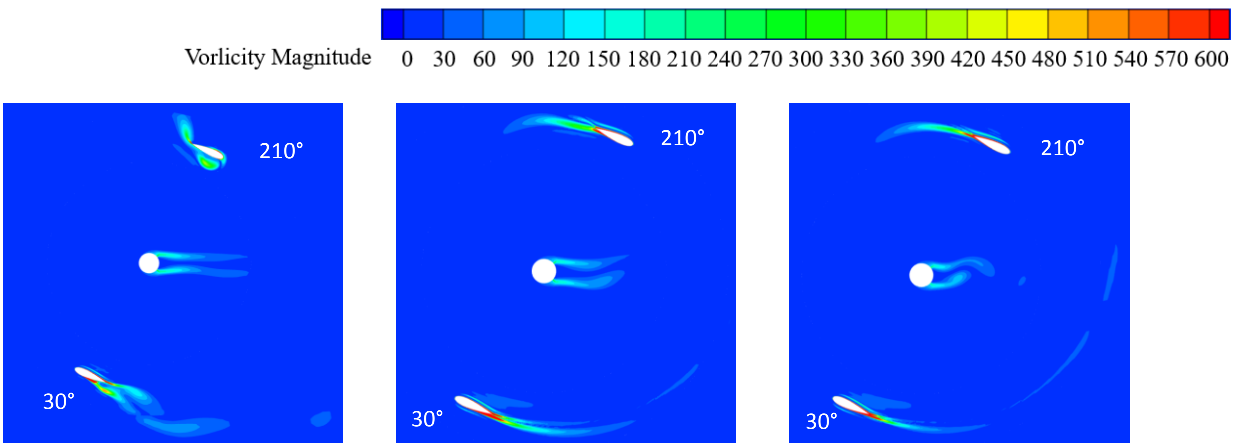

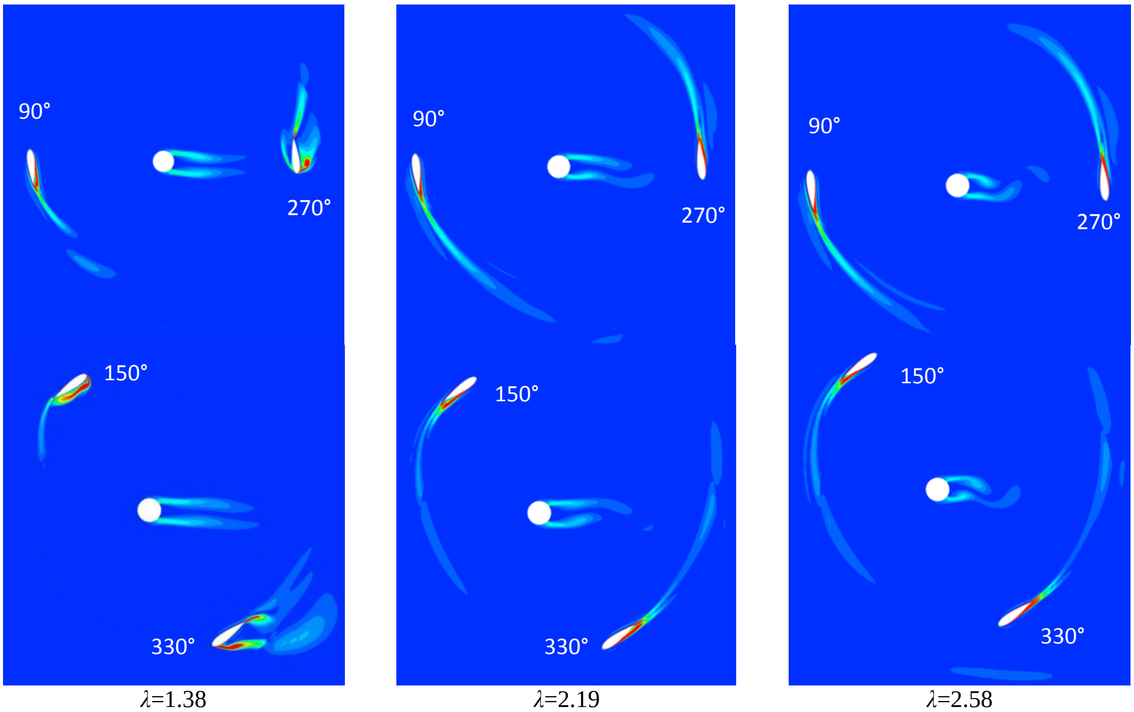

Fig.7 Instantaneous contours of vorticity magnitude on the mid-span section of the blade VAWT

4.4 Comparison of aerodynamic forces

Fig.8 depicts the thrust coefficients (C_{TH}) fluctuation for single blade as a variation of azimuth angle in three cases. As can be seen, the C_{TH} fluctuations of three tip speed ratios have a similar tendency, and the values of the maximum thrust coefficient increase with the growth of tip speed ratio. The maximum thrust coefficients reach 1.58, 1.44 and 1.10 at λ=2.58, 2.19 and 1.38. Furthermore, at the region of [0°, 15°] and [180°, 195°], wind rotor passes the equilibrium position, in which incoming wind speed *U* and blade tangential velocity *V* have the opposite directions, the values of thrust coefficient are all close to 0 for three tip speed ratios.

The fluctuations of tangential force coefficient have similar tendency of torque coefficient, thus that aren't mentioned again in this section. The maximum absolute values of normal coefficient are generated at the azimuth angles 95°, 90° and 90° at λ=2.58, 2.19 and 1.38, and the values are 12.12, 10.85 and 8.27, correspondingly. At the upstream region, the negative normal force occurs at azimuth angle [25°, 180°] in Fig.9, means that the direction of normal force points to the inside of the wind rotor.

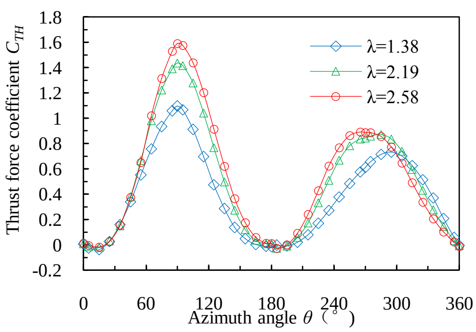

Fig.8 Thrust force coefficient for single blade

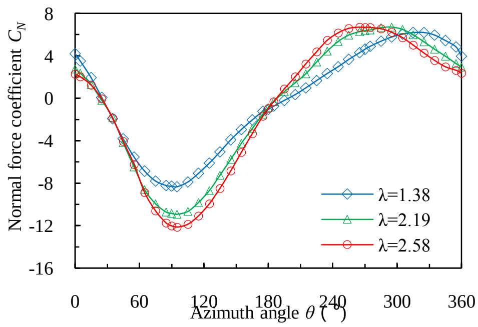

Fig.9 Normal force coefficient for single blade

The evolutions of lift force coefficient for single blade are shown in Fig.10, those values are just opposite to normal force coefficient, meanwhile, the size and location of the maximumabsolutevalue of $C_L$are similar to C_N. The maximum $C_L$are 12.11, 10.97 and 8.6 at λ=2.58, 2.19 and 1.38, and the azimuth angles are angles 95°, 90° and 90°, correspondingly. Fig.11 depicts the fluctuation of drag force coefficient C_D by azimuth angles at three tip speed ratios. The maximum C_D

are all generated at upstream region at θ=90°, and the maximum C_D reach 2.18 at λ=2.58, 2.04 at λ=2.19 and 1.77 at λ=2.58. Furthermore, the C_D peak at upstream region, decreasing with increase of tip speed ratio, are reduced to 0.38 at θ=245°, 0.54 at θ=245°and 0.72 at θ=255° respectively.

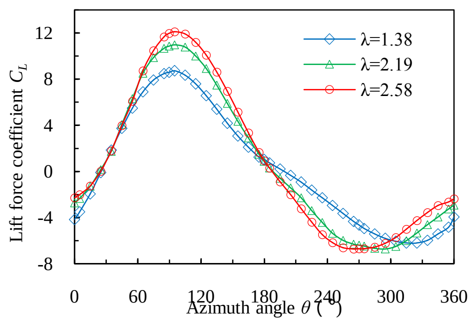

Fig.10 Lift force coefficient for single blade

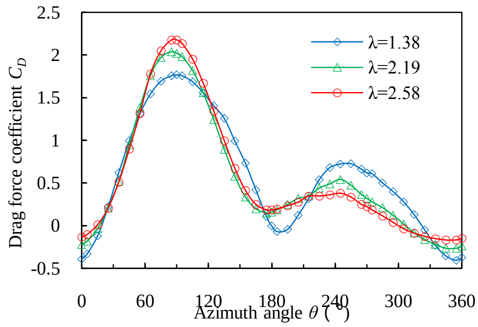

Fig.11 Drag force coefficient for single blade

V. CONCLUSION

Based on CFD simulation technology, this paper analyzes the aerodynamic performance characteristics of linear wing vertical axis wind turbines under different blade tip speed ratios. Some conclusions are shown as follows.

(1) The average power coefficient over one revolution for two blades are 0.051 and 0.116 for the TSRs of 1 and 1.38, respectively. And the maximum average power coefficient is 0.225 for λ=2.19. The dynamic stall occurs in a large azimuth angle at low TSRs, directly affects the flow field and aerodynamic performance of VAWT, which results in lower power output of blades.

(2) Since the attack angle increases as the azimuth angle increases, the flow separation phenomenon on the blade surface also changes gradually, the maximum pressure difference occurs in the upper domain. So the power coefficient and the torque coefficient of wind turbine blade mainly are contributed in upstream.

(3) The torque coefficient and the tangential force coefficient curve corresponding to the three kinds of tip speed ratios are basically the same, and the normal force coefficient, the lift resistance coefficient and the power coefficient curve corresponding to λ=2.19 and λ=2.58 are basically coincident, and λ= 1.38 corresponds to the extreme value. Th better mechanical property of VAWT is occurred at high TSRs, that has similar instantaneous pressure distributions on blades surface and the aerodynamic forces of the rotor shaft.

REFERENCES

[1]. Tummala A, Velamati RK, Sinha DK, Indraja V and Krishna VH. A review on small scale wind turbines. Renewable and Sustainable Energy Reviews. 2016; 56: 1351-1371.
[2]. Chehouri A, Younes R, Ilinca A and Perron J. Review of performance optimization techniques applied to wind turbines. Applied Energy. 2015; 142: 361-388.
[3]. Georgilakis PS. Technical challenges associated with the integration of wind power into power systems. Renewable and Sustainable Energy Reviews. 2008; 12: 852-863.
[4]. Tjiu W, Marnoto T, Mat S, Ruslan MH and Sopian K. Darrieus vertical axis wind turbine for power generation II: Challenges in HAWT and the opportunity of multi-megawatt Darrieus VAWT development. Renewable Energy. 2015; 75: 560-571.
[5]. Dessoky A, Lutz T, Bangga G and Krämer E. Computational studies on Darrieus VAWT noise mechanisms employing a high order DDES model. Renewable Energy. 2019; 143: 404-425.
[6]. Wu G, Zhang L and Yang K. Development and validation of aerodynamic measurement on a horizontal axis wind turbine in the field. Applied Sciences. 2019; 9: 1-21.
[7]. Zhang B, Song B, Mao Z and Tian W. A novel wake energy reuse method to optimize the layout for Savonius-type vertical axis wind turbines. Energy. 2017; 121: 341-355.
[8]. Dessoky A, Bangga G, Lutz T and Krämer E. Aerodynamic and aeroacoustic performance assessment of H-rotor darrieus VAWT equipped with wind-lens technology. Energy. 2019; 175: 76-97.
[9]. Howell R, Qin N, Edwards J and Durrani N. Wind tunnel and numerical study of a small vertical axis wind turbine. Renewable Energy. 2010; 35: 412-422.
[10]. Ragni D, Ferreira CS and Correale G. Experimental investigation of an optimized airfoil for vertical-axis wind turbines. Wind Energy. 2015; 18: 1629-1643.
[11]. Castellani F, Astolfi D, Peppoloni M, Natili F, Buttà D and Hirschl A. Experimental vibration analysis of a small scale vertical wind energy system for residential use. Machines. 2019; 7: 1-19.
[12]. Li Q, Maeda T, Kamada Y, Shimizu K, Ogasawara T, Nakai A and Kasuya T. Effect of rotor aspect ratio and solidity on a straight-bladed vertical axis wind turbine in three-dimensional analysis by the panel method. Energy. 2017; 121: 1-9.

[13]. Li Q, Maeda T, Kamada Y, Murata J, Kawabata T, Shimizu K, Ogasawara T, Nakai A and Kasuya T. Wind tunnel and numerical study of a straight-bladed vertical axis wind turbine in three-dimensional analysis (Part I: For predicting aerodynamic loads and performance). Energy. 2016; 106: 443-452.
[14]. Li Q, Maeda T, Kamada Y, Murata J, Furukawa K and Yamamoto M. The influence of flow field and aerodynamic forces on a straight-bladed vertical axis wind turbine. Energy. 2016; 111: 260-271.
[15]. Zhang T-t, Elsakka M, Huang W, Wang Z-g, Ingham DB, Ma L and Pourkashanian M. Winglet design for vertical axis wind turbines based on a design of experiment and CFD approach. Energy Conversion and Management. 2019; 195: 712-726.
[16]. Elkhoury M, Kiwata T and Aoun E. Experimental and numerical investigation of a three-dimensional vertical-axis wind turbine with variable-pitch. Journal of Wind Engineering and Industrial Aerodynamics. 2015;139: 111-123.
[17]. Li Q, Maeda T, Kamada Y, Murata Junsuke, Furukawa K and Yamamoto M. Aerodynamic models and wind tunnel for straight-bladed vertical axis wind turbines. IOSR Journal of Engineering. 2014; 04: 35-44.
[18]. Maeda T, Kamada Y, Murata J, Yonekura S, Ito T, Okawa A and Kogaki T. Wind tunnel study on wind and turbulence intensity profiles in wind turbine wake. Journal of Thermal Science. 2011; 20: 127-132.
[19]. Thé J and Yu H. A critical review on the simulations of wind turbine aerodynamics focusing on hybrid RANS-LES methods. Energy. 2017; 138: 257-289.
[20]. Abkar M. Theoretical modeling of Vertical-Axis Wind Turbine wakes. Energies. 2018;12: 1-10.
[21]. Almohammadi K, Ingham D, Ma L, Pourkashanian M. CFD sensitivity analysis of a straight-blade vertical axis wind turbine. Wind Engineering. 2012; 36: 571-588.
[22]. Lee Y-T and Lim H-C. Numerical study of the aerodynamic performance of a 500 W Darrieus-type vertical-axis wind turbine. Renewable Energy. 2015; 83: 407-415.
[23]. Li J, Cao Y, Wu G, Miao Z and Qi J. Aerodynamic stability of airfoils in lift-type vertical axis wind turbine in steady solver. Renewable Energy. 2017; 111: 676-687.
[24]. He J, Jin X, Xie S, Cao L, Wang Y, Lin Y and Wang N. CFD modeling of varying complexity for aerodynamic analysis of H-vertical axis wind turbines. Renewable Energy. 2020; 145: 2658-2670.
[25]. Wekesa DW, Wang C, Wei Y and Danao LAM. Influence of operating conditions on unsteady wind performance of vertical axis wind turbines operating within a fluctuating free-stream: A numerical study. Journal of Wind Engineering and Industrial Aerodynamics. 2014; 135: 76-89.
[26]. Shukla V and Kaviti AK. Performance evaluation of profile modifications on straight-bladed vertical axis wind turbine by energy and SpalartAllmaras models. Energy. 2017; 126: 766-795.
[27]. Siddiqui MS, Durrani N and Akhtar I. Quantification of the effects of geometric approximations on the performance of a vertical axis wind turbine. Renewable Energy. 2015; 74: 661-670.